Proceedings of ASME Turbo Expo 2011
GT2011
June 6-10, 2011, Vancouver, British Columbia, Canada

GT2011-45875

MULTISCALE PARTIALLY AVERAGED NAVIER STOKES APPROACH FOR THE PREDICTION OF FLOW IN LINEAR COMPRESSOR CASCADE WITH MOVING CASING

Domenico Borello, Giovanni Delibra and Franco Rispoli
Dipartimento di Ingegneria Meccanica e Aerospaziale
'Sapienza' Università di Roma
Via Eudossiana, 18, 00184 Roma, Italy

ABSTRACT

In this paper we present an innovative Partially Averaged Navier Stokes (PANS) approach for the simulation of turbomachinery flows. The elliptic relaxation k-ε-ζ-f model was used as baseline Unsteady Reynolds Averaged Navier Stokes (URANS) model for the derivation of the PANS formulation. The well established *T-FlowS* unstructured finite volume in-house code was used for the computations.
A preliminary assessment of the developed formulation was carried out on a 2D hill flow that represents a very demanding test case for turbulence models.
The turbomachinery flow here investigated reproduces the experimental campaign carried out at Virginia Tech on a linear compressor cascade with tip leakage. Their measurements were used for comparisons with numerical results.
The predictive capabilities of the model were assessed through the analysis of the flow field. Then an investigation of the blade passage, where experiments were not available, was carried out to detect the main loss sources.

INTRODUCTION

Turbomachinery flows are strongly influenced by the instabilities arising and developing under the influence of various phenomena (adverse pressure gradient, streamlines curvature, etc.) and, ultimately, by the high Re number. Therefore, such class of flows is affected by the presence of strong turbulent phenomena ranging in a very wide spectrum of vortical scales**.** URANS, that is nowadays the most popular numerical approach for turbomachinery design, is not able to capture these instabilities; in fact the Reynolds-Average approach involves an ensemble-averaging operation which models any turbulent phenomena having a characteristic scale that is below the turbulent time or length scales. Limitations of URANS have to be related to the crude assumptions on which most of the popular models usually applied for turbomachinery design (i.e. eddy viscosity models - EVM) are developed. Therefore, it is quite evident that the URANS models based on eddy viscosity closure cannot capture the true physics of such flows, as they cannot resolve the main vortical structures and recover the real flow unsteadiness. Typical drawbacks in the simulation of a linear compressor cascades are the correct prediction of the tip leakage or hub vortices generation and development. On the other hand, Large Eddy Simulation (LES) represents the best option to scrutinize the physics of turbulent flows, but (at least for industrial applications) it requires an enormous computational load in terms of grid and time resolution, while coarse LES solutions can return worst-than-URANS results. In order to improve URANS performance in the prediction of turbomachinery flows many efforts have been recently made, including the development of models tuned to solve a particular class of phenomenology on a given geometry. Current developments on turbomachinery Computational Fluid Dynamics (CFD) focus on the improvement and testing of advanced RANS models within the 3D URANS framework (e.g. Craft et al. [1]), on Reynolds Stress Models (RSM) computations [2-4], on the hybridization of advanced near-wall RANS models with LES applied away from solid walls [5] or on sensitising URANS to instabilities with different strategies [6-7]. These approaches opened new niches for the use of URANS when an accurate description of flow anisotropy and other complex features is required. We present here the application of k-ε-ζ-f elliptic-relaxation model [8, 9] reformulated in Partially-Averaged Navier-Stokes (PANS) framework, that allows to dynamically modulate the averaging cutoff filter to pass from URANS to Direct Numerical Simulation (DNS). With respect to other hybrid methods, PANS proposes a reformulation of the closure equations that involves not only a modification in the source terms like for example Detached Eddy Simulation (DES), but also a change in the diffusion terms of the closure equations that is able to smear out all the possible peaks of the transported variables, allowing a

smooth passage from URANS to DNS. A key aspect of this process is that the turbulent (here called "unresolved") viscosity acting in the momentum equation is lower than the one that is used in closure equations due to a modification introduced in the turbulent Prandtl number. This approach drastically reduces the weight of the model allowing to sensitize the simulation to physical instabilities that are responsible for the unsteadiness of the flow. This model, that was assessed on simplified geometries adopting different baseline URANS models [7], [10], is here applied to solve the flow in a linear (3D) compressor cascade with moving endwall. The aim of the present work is to analyze the secondary motions and losses in the blade passage and in the wake, that are influenced by the sliding of the casing; such motions are cause of losses, noise and vibrations and therefore their physics needs to be understood. Experimental database is provided by the study of Devenport and co-workers at Virginia Tech - see e.g. [11,12].
In the following the PANS approach is briefly described and an assessment of the turbulence model is carried out with reference to a well known (2D hill) test case. In the results section we analyze the turbomachinery configuration and compare the PANS results with available measurements and the parent URANS model. Some conclusion will be drawn at the end.

PANS MODEL

PANS is a "second generation" URANS method recently proposed by Girimaji [7] following the original idea of Speziale [13] to develop a new approach for turbulence modelling, able to switch from URANS to LES to DNS by changing the averaging filter-width. Therefore, PANS model is basically a URANS model where the averaging procedure is only partial and regulated by a filter parameter (f_i) equal to the ratio of the unresolved and total i turbulent variable.
It is important to point out that the quality of PANS results is strongly related to the characteristics of the baseline URANS model. In fact, where the resolved turbulence is negligible when compared with the modelled one, an accurate turbulence model has to be used to reproduce the flow behaviour. Furthermore, if compared with LES sub-grid scale models, the URANS models are based on more complex assumptions that allow to better reproduce the physics of turbulence when the turbulent length scale of the resolved motion is out from the inertial sub-range and then strong non-equilibrium conditions are in play.
This implies that even if any URANS model can be chosen to derive the corresponding PANS formulation, the adoption of an advanced URANS closure must be considered to analyze complex flows as in turbomachinery.
In the present work, a PANS implementation of the elliptic-relaxation k-ε-ζ-f model [8] is proposed. This model is based on the elliptic-relaxation concept [14] and introduces two additional variables to the classical two-equations eddy viscosity closure. The first, ζ, represents the ratio between the normal-to-the-wall component of the Reynolds Stress, vv, and k. This variable is able to account for the anisotropic behaviour of the Reynolds stresses near the wall (where $vv \propto y^4$, while the other normal stresses and k are proportional to y^2). Moreover, the adoption of the k-ε-ζ-f model avoids the introduction of damping functions in the equations of the turbulent variables and eddy viscosity when the near-to-the-wall region is approached.
The second variable, f, is introduced in order to take into account the non local influence of pressure reflection. Further details on the formulation can be found in [8]. In analogy with the PANS formulation derived from Girimaji [7] for a k-ε model, we adopt here an approach based on two filter parameters:

$$f_k = \frac{k_u}{k} \qquad f_\varepsilon = \frac{\varepsilon_u}{\varepsilon} \tag{1}$$

where the subscript "u" stands for "unresolved" part. The unresolved part is modelled using the standard k-ε–ζ-f model. From (1) it is straightforward that for f_k=f_ε=1.0 the model recovers a full URANS behaviour as k and ε are totally unresolved, whereas for f_k=f_ε =0.0 all the scales of the motion are resolved and the model acts as DNS. The filter width f_k should vary with the space, however we experienced that the spatial variation of the coefficient could lead to unphysical solutions when very complex flow were analysed. In agreement with Girimaji [7] we assumed a constant value of f_k. The same comments can be made for the ε equation. However, we have to note that most of the dissipation occurs at the small scales (comparable to Kolmogorov scales); the solution of these scales of motion is simply not affordable for the simulation of complex flows. Therefore it is not possible to resolve any dissipation scale and consequently we assume f_ε=1, so that the dissipation is completely modelled.
Finally, we assumed that the ζ and f variables can be filtered using the same parameter f_k adopted for the turbulent kinetic energy.
The set of equations describing the incompressible PANS k–ε–ζ–f closure reads:

$$\frac{\partial U_k}{\partial x_k} = 0 \tag{2}$$

$$\frac{\partial U_i}{\partial t} + U_k \frac{\partial U_i}{\partial x_k} = -\frac{1}{\rho}\frac{\partial P}{\partial x_i} + \frac{\partial}{\partial x_k}\left[\left(\nu + \nu_u\right)\frac{\partial U_i}{\partial x_k}\right] \tag{3}$$

$$\nu_u = c_\mu \zeta_u k_u \tau \tag{4}$$

$$\frac{Dk_u}{Dt} = P_u - \varepsilon_u + \frac{\partial}{\partial x_j}\left[\left(\nu + \frac{\nu_u}{\sigma_{ku}}\right)\frac{\partial k_u}{\partial x_j}\right] \tag{5}$$

$$\frac{D\varepsilon_u}{Dt} = C_{\varepsilon 1} P_u \frac{\varepsilon_u}{k_u} - C^*_{\varepsilon 2}\frac{\varepsilon_u^2}{k_u} + \frac{\partial}{\partial x_j}\left[\left(\nu + \frac{\nu_u}{\sigma_{ku}}\right)\frac{\partial \varepsilon_u}{\partial x_j}\right] \tag{6}$$

$$\frac{D\zeta_u}{Dt} = f_u - \frac{\zeta_u}{k_u}\left[P_u\right] + \frac{\partial}{\partial x_j}\left[\left(\nu + \frac{\nu_u}{\sigma_{ku}}\right)\frac{\partial \zeta_u}{\partial x_j}\right] \tag{7}$$

$$L^2\nabla^2 f_u - f_u = \frac{1}{T_u}\left(c_1 + C_2' \frac{P}{\varepsilon}\right)\left(\zeta_u - \frac{2}{3}\right) \tag{8}$$

$$C^*_{\varepsilon 2} = C_{\varepsilon 1} + f_k (C_{\varepsilon 2} - C_{\varepsilon 1}) \tag{9}$$

The main novelty of PANS is that the eddy viscosity (4) is now smaller than in the original URANS as it is computed on the basis of the unresolved part only.

On the other hand, Girimaji demonstrated [7] that the Prandtl coefficient in the eqs. (5-7) becomes:

$$\sigma_{ku} = \sigma_k \frac{f_k^2}{f_\varepsilon} \tag{10}$$

This means that the turbulent (unresolved) eddy viscosity acting in closure equations is different from (and greater than) the one used for the momentum equation. This implies that the momentum equation is sensitized to flow unsteadiness via the reduction of the turbulent viscosity, while the turbulent variables variation is strongly smoothed by the increased eddy viscosity.

COMPUTATIONAL DETAILS

The finite volume unstructured in-house code *T-FlowS* was used for computations. The code was originally developed at TU Delft and now it is advanced in our group at Sapienza Università di Roma. The code is second order accurate in space and time. Semi-Implicit Method for Pressure Linked Equations (SIMPLE) algorithm is adopted for the coupling of pressure and velocity fields, using CDS convective scheme on momentum equation and Sharp and Monotonic Algorithm for Realistic Transport (SMART) on the other transport equations for PANS computations. For URANS calculations SMART scheme is applied on all the equations. Preconditioned Conjugate Gradient algorithm is used as a solver of the algebraic system. For the details of the implementation of the solver see Niceno and Hanjalić [15].

NUMERICAL CAMPAIGN

Assessment of the adopted PANS formulation

Assessment of PANS methodology was carried out on the very well known turbulence modelling test case of 2D periodic hill at Re=10,595 (based on the hill height h, bulk velocity U_b and fluid viscosity) comparing experimental data available from PIV measurements [16]. All the variables were normalized on the basis of the reference values used for calculating the Reynolds number. The geometry is sketched in Fig. 1. Vertical lines indicate the measurement sections. Periodicity was assumed in streamwise (x) and spanwise (z) directions and a constant mass flow was set in streamwise direction; on the upper and lower walls no-slip conditions were imposed. The computational domain extended for 4.5 z/h in spanwise direction. The domain was discretised with 250x80x32 cells, with a near-wall clustering sufficient to ensure y^+<1.0 on each wall. A non dimensional time step of 0.01 was enforced to obtain a CFL number always lower than 1. The residual threshold was set equal to 10^{-7} for all the variables and to 10^{-5} for the SIMPLE algorithm.

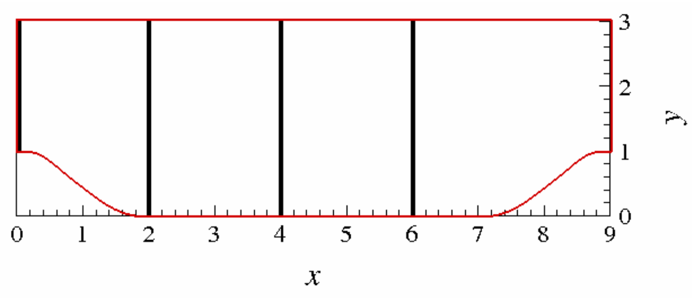

Fig. 1 – Sketch of the 2D hill geometry. Vertical lines refer to the control sections used in the discussion, corresponding to separation (x=0.05), recirculation (x=2.0), reattachment (x=4.0) and straight duct (x=6.0).

To get a stable PANS solution of hill flow, it was necessary to tune the initial conditions. A first attempt to start with a steady-state URANS solution led to a (coarse) DNS (as ν_u went to zero everywhere) and to a subsequent flow laminarisation. It is important to note that the parent URANS simulation always returned a steady two-dimensional flow, as all the other linear EVM. In order to have a suitable initial field, URANS ζ-f velocity field was periodically perturbed with random fluctuations; this allowed the field to become fully three-dimensional, even if it completely destroyed the field of k_u. For this reason k_u had to be reset to a constant value of 0.001 everywhere and let evolve according to (5) again. As at this time coherent structures were already present in the field it was possible to sustain a k_u field and to obtain a numerically stable computation with a fully three-dimensional unsteady field. In order to obtain a statistically convergent solution, the time averaging procedure was carried out for 40 flow through times (FTT). The final results were then averaged over the 32 spanwise planes.

A preliminary analysis of the PANS sensitivity to filter width was carried out adopting two different values of f_k as in [10].

Looking at the results in terms of turbulent (unresolved) viscosity normalized with molecular viscosity in Fig. 2 it is evident that passing from f_k=0.4 to f_k=0.5 the ν_u value becomes three times larger.

In Table 1 the position of the separation and reattachment points is reported for experiments and computations. PANS with f_k=0.5 returned the best agreement with experimental results.

Looking at streamwise x (Fig. 3) and wall-to-wall y (Fig. 4) velocity profiles, PANS ζ-f with f_k = 0.5 returned an overall better prediction of velocity profiles, and in particular they correctly reproduced separation and reattachment, as said before; the same model with f_k = 0.4 showed a slight delay in the inception of separation and in reattachment.

Table 1: Position of the separation and reattachment points

	separation (x/h)	reattachment (x/h)
experiments	before 0.5	4.00
URANS	0.22	4.50
PANS (f_k=0.4)	0.23	4.30
PANS (f_k=0.5)	0.20	4.15

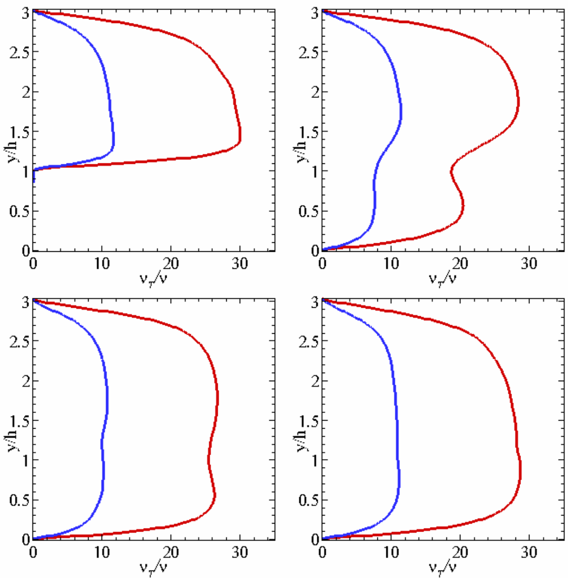

Fig. 2 – Time-averaged ν_u/ν profiles at x/h=0.05, x/h=2.0, x/h=4.0 and x/h=6.0. Red: f_k=0.4, Blue: f_k=0.5.

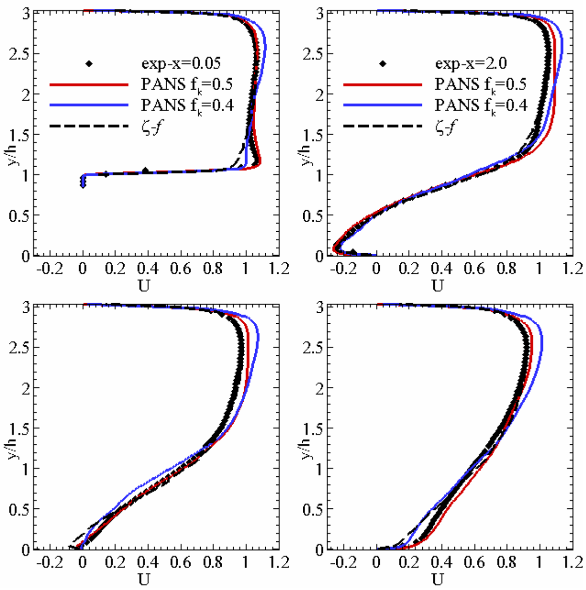

Fig. 3 - Time-averaged streamwise velocity profiles at x/h=0.05, x/h=2.0, x/h=4.0 and x/h=6.0. Red: f_k=0.4, Blue: f_k=0.5.

The same behaviour was recognizable when using a PANS approach developed from *k-ε* model [10] which showed an overall worst prediction if compared with *k-ε-ζ-f* (not shown here).

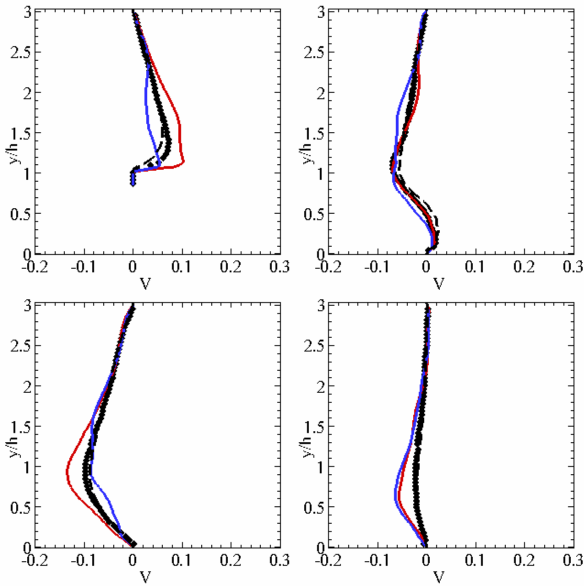

Fig. 4 – Time-averaged wall normal velocity profiles at x/h=0.05, x/h=2.0, x/h=4.0 and x/h=6.0. Red: f_k=0.4, Blue: f_k=0.5.

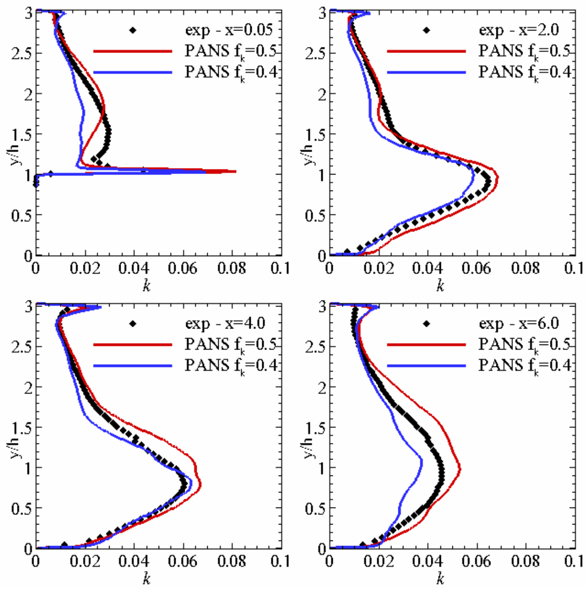

Fig. 5 – Time-averaged turbulent kinetic energy profiles at x/h=0.05, x/h=2.0, x/h=4.0 and x/h=6.0. Red: f_k=0.4, Blue: f_k=0.5.

In Fig. 5 we compared the profiles of turbulent kinetic energy measured by Rapp [16] using 2D PIV with the computed total kinetic energy profiles. Fig. 5 shows that the adoption of a higher value of f_k allows to reconstruct a better prediction of the turbulent field. However, despite the very strong differences in turbulent viscosity shown in Fig. 2, the two computations demonstrated a certain agreement. This was due to the fact that in both cases the modelled part of *k* is considerably smaller with respect to the resolved contribution and therefore its influence on the overall flow was negligible.

Simulation of a 3D compressor cascade with tip leakage

In an ongoing project we are analyzing the flow in a 3D linear compressor cascade, experimentally studied at Virginia Tech University in the group of Prof. Devenport using three-orthogonal velocity component fiber optic laser Doppler anemometer (see e.g. [11-12]). The blade had a GE rotor B profile. In previous papers [17-18] we scrutinized the quality of the predictions of different turbulence models at different heights of the blade tip. Other details about the experimental setup or the simulations can be found there. Here we simply say that the chord of the blade was equal to 254 mm, the bulk inflow velocity magnitude U_b was 26 m/s, the solidity was 1 and the ensuing Reynolds number was $4x10^5$. The tip height was equal to 1.65% of chord (see Fig.6). All the variables were normalized using the cited parameters. The computational grid consisted of ~3.6 millions cells. A region of hexahedra was used all around the blade surface while the rest of the domain was filled with triangular prisms (see Fig. 7). The tip leakage region was discretised using 20 equally spaced grid cells in the normal-to-the-casing direction (z). The grid refinement was sufficient to guarantee a y^+ value lower than 3 in almost all the cells placed in the layer adjacent to the walls, except for a very small amount (less than 0.1%) placed in regions were the flow separated. The same mesh was used for previous computations and it was considered adequate [17].

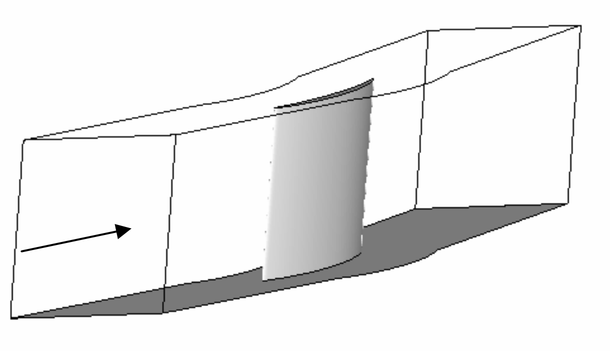

Fig. 6 – Compressor cascade: computational domain: the arrow indicates the inflow direction

The set of boundary conditions used for the URANS computations [17] was the same of PANS simulations: we imposed undisturbed constant inflow conditions aligned with experimental measurements, no-slip conditions on the solid walls and convective boundary conditions at the outlet. The turbulent variables were tuned in order to guarantee that the boundary layer thickness in the mid of the blade passage and at X/c_a=0 (see Fig.8) was equal to the measured value. In the two limiting surfaces placed in pitchwise direction we imposed periodicity to simulate the presence of an infinite number of blades.
The residual threshold was set to 10^{-7} for all the variables and to 10^{-5} for the SIMPLE iterative algorithm. To study the exclusive influence of relative motion between blade and casing, neglecting the effect of Coriolis force, a moving belt aligned with the cascade blades was placed to simulate the casing motion. The belt velocity was set equal to 0.9077 U_b (see Fig.8). The time step used was equal to $2x10^{-4}$ and 4.5 flow through times were simulated to obtain time-averaged results.
The parameter f_k was set equal to 0.5.

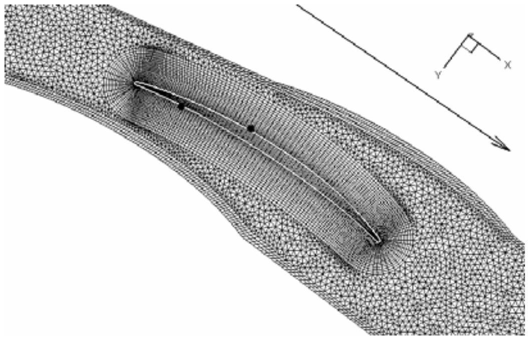

Fig. 7 – Compressor Cascade: details of the tip region

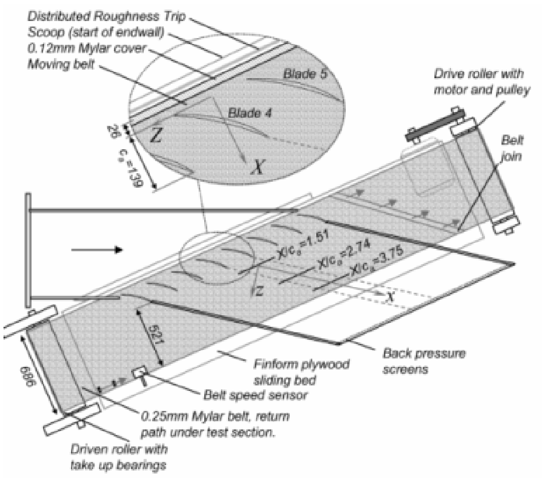

Fig. 8 – Measurement test rig with moving casing [12]

A preliminary analysis of the tip leakage flow is shown in Fig. 9, where instantaneous value of Q-factor and pressure laplacian ($\nabla^2 p$) isosurfaces are used to identify the turbulent structures in the tip gap. Q factor represents the balance between the instantaneous values of rotation and strain rate (11) and it is then able to identify the vorticity induced by the turbulent motion separating it by the geometry-induced vorticity (e.g. boundary layer).

$$Q = \frac{1}{2}\left(\Omega_{ij}\Omega_{ij} - S_{ij}S_{ij}\right) \tag{11}$$

The Q factor isosurface shows the presence of large perturbed region near the tip leakage. Upstream of the leading edge and in the first portion of the suction side a corrugation of the surface indicates the possible presence of pressure fluctuations. Moving downstream, the generation and development of the tip leakage vortex induced a deep perturbation of the Q=40 isosurface (extending up to the pressure side) and a strong increase of the Q factor magnitude. Downstream of the trailing edge the footprint of the wake is clearly visible. The streamlines pattern shows that the casing motion drags the tip leakage vortex in pitchwise direction crossing the blade passage and moving towards the pressure side. Furthermore, both streamlines and pressure laplacian distribution show that on the suction side, under the tip leakage vortex, other turbulent vortical structures exist, developing close to the suction side possibly mixing with the wake immediately downstream to the trailing edge.

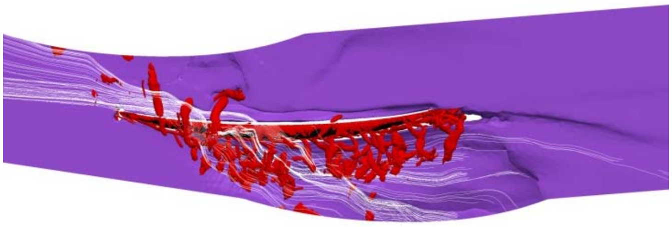

Fig. 9 – Compressor cascade: instantaneous vortical structures near the tip: blue surface Q=40, red surface $\nabla^2 p$=600, white lines instantaneous streamlines.

In Fig. 10 the strong influence of the casing motion on the tip leakage vortex in a cross section at 1.51 c_a downstream from the leading edge of the blade (see small sketch on the right) is highlighted. Furthermore, in the steady case a different colour bar was used. The streamwise velocity contours put in evidence that the tip leakage vortex is swept from the suction surface along all the blade passage and then reaches the pressure side where it is subjected to a mixing and a strong interaction with the wake.

Numerical results show that the tip-leakage vortex is closer to the blade and to the wall and the velocity defect is smaller than in experiments. PANS and URANS simulations show a qualitative agreement, even if PANS returns a more pronounced velocity defect in the tip leakage vortex, a thicker boundary layer as well as a more accurate detection of the vortex core position. On the other hand, URANS shows a smoothed velocity field, indicating an excessive contribution of the added turbulent viscosity.

The experimental turbulent kinetic energy contour (Fig.11) shows a large turbulent core near the wall where the tip leakage vortex interacts with the blade wake. In the suction side (right of the wake in Fig.11) the low turbulent region extends very close to the wall. In the numerical results total kinetic energy profiles are shown. PANS computations return a close agreement with experiments, correctly predicting the position of the region of maximum k and its magnitude, the wake and the low turbulent region on the suction side. It is worth noting that the destruction of eddy viscosity induced by the partially averaging procedure allowed to reasonably predict the strong unsteadiness generated by the turbulent structures. Consequently, we obtained an accurate distribution of the total (modelled + resolved) turbulent kinetic energy k.

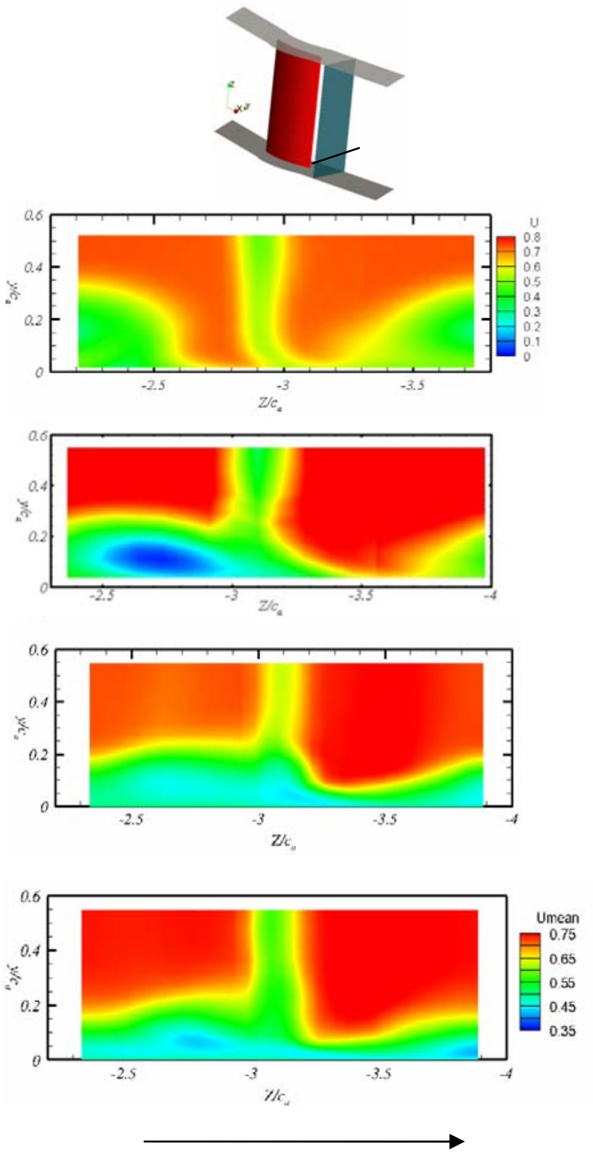

Fig. 10 – Time-averaged velocity contours in a cross-section in the wake of the tip leakage (1.51 c_a from the leading edge); from top to bottom: sketch of the measuring section in the wake (the measurement section is the one below the black line), experiments with steady casing, then experiments, PANS and URANS with moving casing. The black arrow indicates the casing motion direction.

On the other hand, the turbulent kinetic energy in the wake was smoothed and the shape of k profiles in the tip leakage was not perfectly predicted. URANS computations over-predict the k value along all the casing region and especially in the tip leakage vortex core. This is probably due to a double accounting of turbulence in this region as the k averaged field is computed summing up the modelled k and the resolved contribution. To clarify this aspect we reconstructed the URANS solution neglecting the resolved contribution: even so the model was not able to reproduce an appropriate turbulent kinetic energy profile (not shown here).

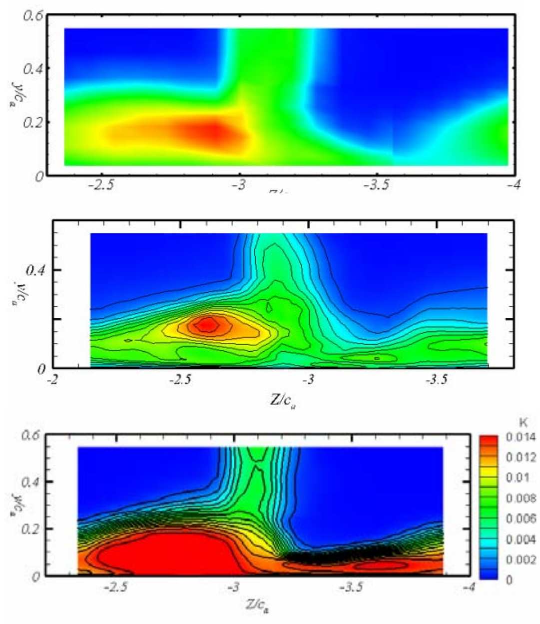

Fig. 11 – Time-averaged turbulent kinetic energy contours in a cross-section in the wake of the tip leakage (1.51 c_a from the leading edge); top: experiments, centre: PANS; bottom: URANS.

Experimental database did not give any information about the flow in the blade passage. It is therefore interesting to investigate the main phenomena arising there in order to identify the possible sources of losses.

In Fig.12 the loss coefficient ξ:

$$\xi = \frac{\left(P_{01} - P_{0i}\right)}{\frac{1}{2}\rho U_b^{\,2}} \tag{12}$$

distribution along several planes normal to the chord is shown. The losses are concentrated in the wake region, near the hub and the casing walls. In particular, the interaction between the hub and the suction side boundary layers led to a strong increase of the losses that is clearly visible in the fourth reference plane, that is placed in the blade passage and near the trailing edge. This phenomenon is still visible in the wake. The interaction between the casing and the tip leakage vortex is recognizable from the increase of the loss coefficient near the casing itself. In all the sections the maximum value of such coefficient is located in the center of the tip-leakage vortex.

In Fig.13, the streamline velocity contours are shown. URANS and PANS simulations are compared with the results of a similar configuration with non-moving casing.

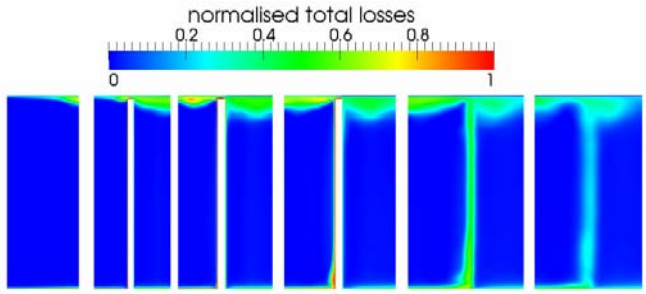

Fig. 12 – Distribution of ξ along several planes. The position of the six planes are shown below in Fig.15.

As said above, the relative motion between the casing and the blade sweeps the tip leakage vortex away from the suction surface. This has a stabilizing effect on the pressure distribution on the suction side (Fig.14) and, consequently, the developing hub vortex is very weak and it has only a limited impact on the wake flow. This behavior is quite similar for both simulations.

It is quite interesting to notice that, when there is no relative motion between the casing and the blade, the flow inside the blade passage is strongly disturbed by the position of the tip leakage vortex. In fact, the presence of a strong rotating structure placed near the suction side, aspirating flow from below, fosters the generation of the hub vortex. This phenomenon is strongly evident in the URANS simulation (and it is shown by the red ellipse in Fig. 14) where the smoothing effect of the eddy viscosity maintains the tip leakage vortex very close to the suction surface and consequently a very strong hub vortex is generated.

In Fig. 15 the PANS time-averaged velocity components in reference sections normal to the chord, placed upstream of the leading edge, in the blade passage and in the wake are shown.

The plots of the streamwise and the spanwise normal-to-the-casing velocity components clearly show the presence of a vertical motion near the hub developing in an hub vortex in the second half of the blade and still evident in the wake far from the leading edge.

Finally, the unsteady behavior of the flow in the blade passage was investigated. In Fig. 16 the instantaneous and time average streamwise velocity fields in the same reference section of Fig.12 are shown.

The flow shows strong unsteadiness induced by the generation of the tip leakage vortex, starting from the third reference section. Moving downstream, the unsteadiness increases and reaches a maximum value in the first wake section just downstream the trailing edge where also the imprint of the hub vortex is clearly visible. The presence of this structure is also confirmed by the spanwise velocity contours (also shown in time averaged results in Fig. 15) showing two very close regions with velocity component having opposite sign.

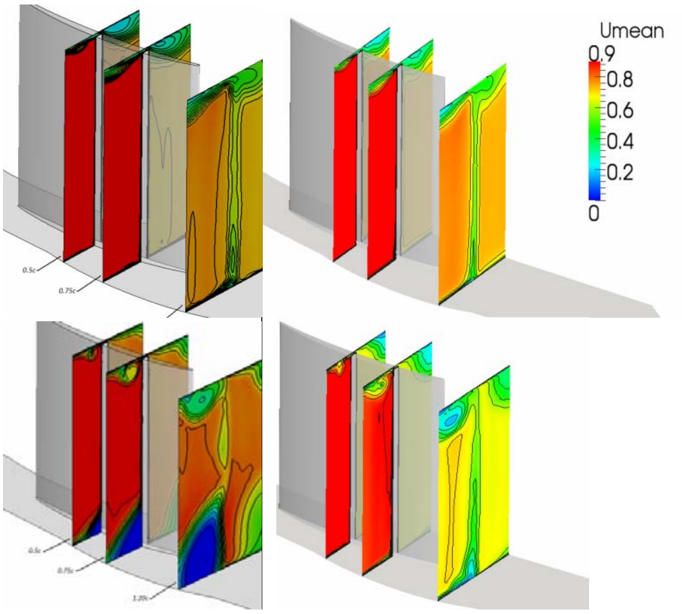

Fig. 13 – Time-averaged streamwise velocity contours in three different cross-sections placed in the aft part of the blade and in the wake; top: moving casing, bottom: steady casing; left: URANS; right: PANS.

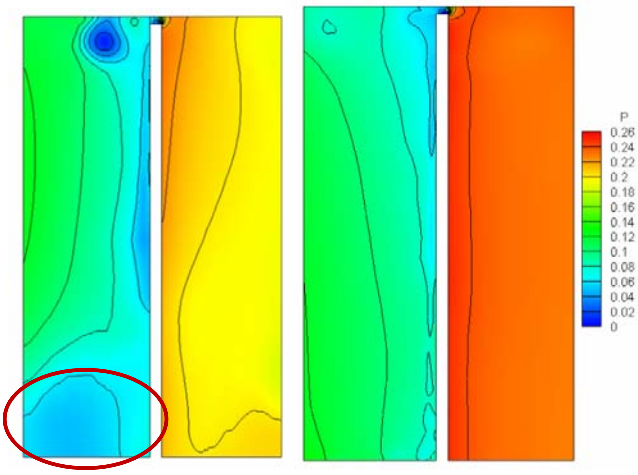

Fig. 14 – Time-averaged pressure contours in a section near the trailing edge (95% c_a): left – steady casing; right: moving casing

CONCLUSIONS

We investigated the flow field developing in a linear 3D compressor cascade with a moving casing mimicking the real phenomena arising in rotating turbomachinery. This configuration allowed to analyze the influence of the relative motion of the blade and the casing neglecting the influence of Coriolis and centrifugal forces.
An innovative Partially Averaged Navier Stokes approach was used for the computations with the aim to capture part of the

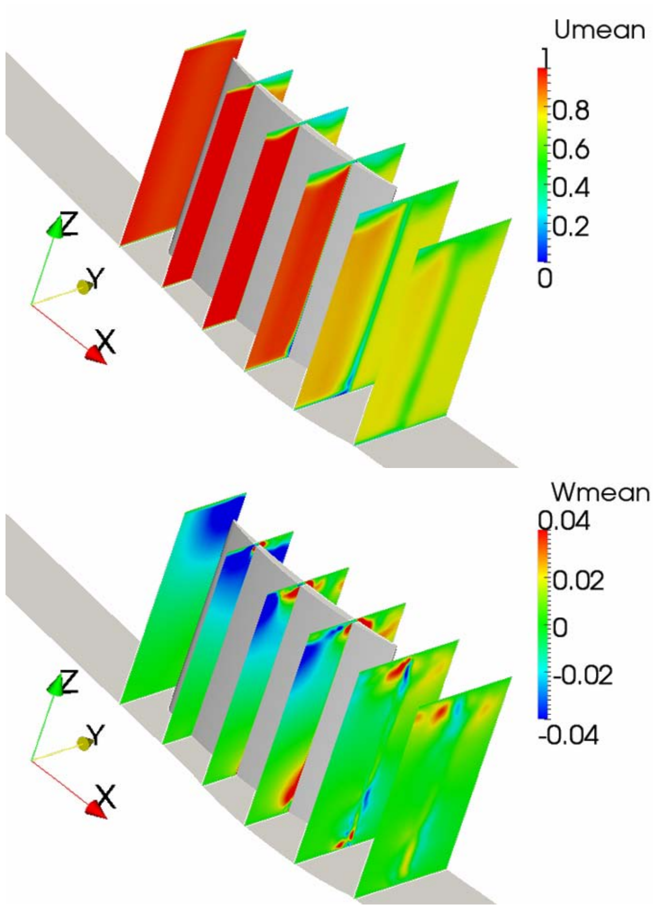

Fig. 15 – Streamwise (top) and normal to the casing (bottom) mean velocity contours in six different cross sections.

flow unsteadiness, reducing the importance of the modeled turbulent field and consequently the magnitude of the (added) turbulent viscosity.
The PANS approach demonstrated to be able to reproduce the main flow features in both a calibration test case as well as in the examined turbomachinery configuration.
The analysis of the flow field showed the influence of the casing motion on the development of the secondary flows. In fact, it was demonstrated that the sweeping of the tip leakage vortex far from the suction side allows to strongly reduce the losses related to the hub vortex structures, even if the influence of wake and tip leakage vortices remain evident. Furthermore, the PANS approach demonstrated to be able to reproduce the flow unsteadiness related to strong unstable loss phenomena.

NOMENCLATURE

latin

c_a	axial chord
CDS	central difference scheme
f	elliptic relaxation function
f_ε	PANS dynamic filter parameter for ε eqn
f_k	PANS dynamic filter parameter for k eqn
k	turbulent kinetic energy

$l=k^{3/2}/\varepsilon$ turbulent length scale
P_{01} total pressure in inlet sections
P_{02} total pressure in outlet sections
P_{0i} total pressure in current position
P_u production of unresolved turbulent kinetic energy
TI turbulence intensity
U_b bulk velocity
vv normal to the wall Re stress component
y wall distance

greek
ε dissipation of turbulent kinetic energy
ζ closure quantity that tends to vv/k near the solid walls
σ_i Prandtl number for "i" variable
σ_{iu} Prandtl number for the unresolved part of "i" variable
ξ Total loss coefficient
subscripts
u unresolved part of the turbulent variables

ACKNOWLEDGMENTS

The authors want to thanks Prof. Hanjalić for the very useful discussions about the development and implementation of k-ε–ζ-f PANS formulation.

Computations were carried out on the CASPUR Matrix Cluster under the Caspur HPC Grant 2010.

REFERENCES

[1] Craft, T.J., Launder, B.E. and Suga, K., 1996, "Development and application of a cubic eddy-viscosity model of turbulence", Int. J. of Heat and Fluid Flow, **17**, pp. 108-155.
[2] Hanjalić, K., and Jakirlić, S., 1998, "Contribution Towards the Second Moment Closure Modelling of Separating Turbulent Flows", Computers and Fluids, 27(2), pp.137-156.
[3] Borello, D., Hanjalić, K., and Rispoli, F., 2007, "Computation of tip-leakage flow in a linear compressor cascade with a second-moment turbulence closure" , Int. J. of Heat and Fluid Flows, **28** (4), pp. 587-601.
[4] Gerolymos, G. A. and Vallet, I., 2007, "Robust Implicit Multigrid Reynolds-Stress Model Computation of 3D Turbo-machinery Flows", Journal of Fluids Engineering, 129(9), pp. 1212-1227.
[5] Delibra, G., Hanjalić, K., Borello, D., and Rispoli, F., 2010, "Vortex structures and heat transfer in a wall-bounded pin ma-trix: LES with a RANS wall-treatment" , Int. J. of Heat and Fluid Flow, 31, pp. 740–753.

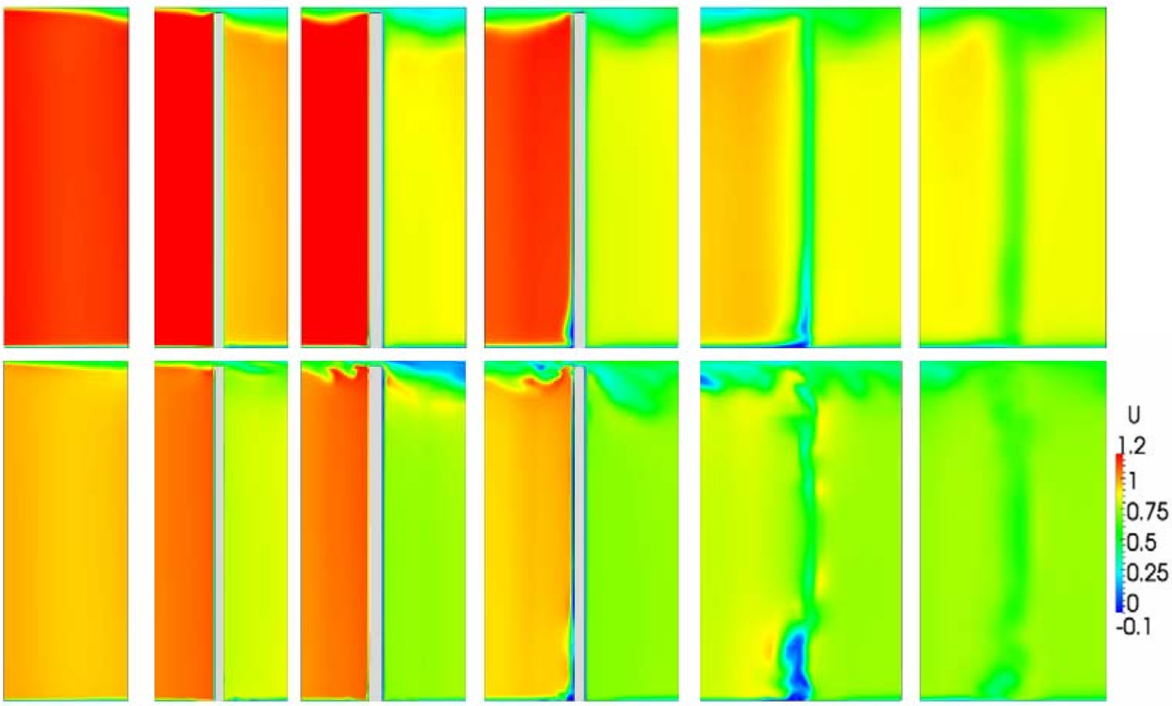

Fig. 16 –Streamwise PANS velocity contours in six reference sections indicated in the right bottom sketch; top: time-averaged field, bottom: instantaneous field.

[6] Menter, F.R., and Egorov, Y., 2010 "The Scale-Adaptive Simulation Method for Unsteady Turbulent Flow Predictions. Part 1: Theory and Model Description", Flow, Turbulence and Combustion, 85(1), pp.113-138.

[7] Girimaji, S. S., 2006, "Partially-Averaged Navier-Stokes Model for Turbulence: A Reynolds-Averaged Navier-Stokes to Direct Numerical Simulation Bridging Method", Journal of Applied Mechanics, 73, pp 413-421.

[8] Hanjalić, K., Popovac, M., and Hadziabdić, M., 2004, "A robust near-wall elliptic-relaxation eddy viscosity turbulence model for CFD", Int. J. of Heat and Fluid Flow, 25(6), pp. 1047-1051.

[9] Borello D., and Orlandi P., 2011, "DNS scrutiny of the z-f elliptic-relaxation eddy-viscosity model in channel flow with a moving wall", Flow, Turbulence and Combustion, 86, pp. 295-309.

[10] Ma, J.M., Peng, S.-H., Davidson, L., and Wang, F., 2010, "A low-Re number Partially-Averaged Navier-Stokes model for turbulence", Proceedings of ETMM8, Marseille, France, 2010.

[11] Muthanna, C., and Devenport, W.J., 2004, "Wake of a Compressor Cascade with Tip Gap, Part 1: Mean Flow and Turbulent Structure", AIAA Journal, 42(11), pp. 2320-2331.

[12] Wang, Y., and Devenport, W.J., 2004. "Wake of a compressor cascade with tip gap, Part2: effects of endwall mo-tion", AIAA Journal, 11, pp. 2332-2340.

[13] Speziale, C., G, 1996, "Computing non-equilibrium flows with time-dependent RANS and VLES", 15th ICNMFD.

[14] Durbin, P. A., 1991, "Near wall turbulence closure modelling without damping functions", Theor. Comp. Fluid Dynamics, 3, pp. 1-13.

[15] Niceno, B., and Hanjalić, K., 2005, "Unstructured large-eddy- and conjugate heat transfer simulations of wall-bounded flows", in M. Faghri and B. Sunden (Eds) Modeling and Simulation of Turbulent Heat Transfer, (Developments in Heat Transfer Series), WIT Press, pp. 1-40.

[16] Rapp, C., 2008, "Experimentelle Studie der turbulenten Stromung uber periodische Hugel", Dissertation, Technische Universitt Munchen.

[17] Borello, D., Delibra, G., Hanjalić, K., and Rispoli, F., 2010, "Hybrid LES/RANS study of turbulent flow in a linear compressor cascade with moving casing", Proceedings of ASME Turbo Expo 2010: Power for Land, Sea and Air GT2010 June 14-18, 2010, Glasgow, UK GT2010-23755.

[18] Borello, D., Delibra, G., Hanjalić, K., and Rispoli, F., 2009, "URANS and Hybrid LES/RANS Computations of Tip Leakage and Secondary Flows in Axial Compressor Cascade" , Proceedings IMechE Part A: Journal of Power and Energy, 223, pp. 645-655.